AFRL-SR-AR-TR-07-0401

REPORT DOCUMENTATION PAGE

1. REPORT DATE (DD-MM-YYYY)	2. REPORT TYPE	3. DATES COVERED (From - To)
16-04-2007	Final Technical Report	06-01-2002 to 15-11-2006

4. TITLE AND SUBTITLE

Quasi-Phasematched Nonlinear Optics: Materials and Devices

5a. CONTRACT NUMBER

5b. GRANT NUMBER
F49620-02-1-0240

5c. PROGRAM ELEMENT NUMBER

6. AUTHOR(S)

M.M. Fejer, R. Gaume, J. Huang, D. Hum, P. Kuo, R. Roussev, R. Route
A. Schober, J. Wisdom, and X. Xie

5d. PROJECT NUMBER

5e. TASK NUMBER

5f. WORK UNIT NUMBER

7. PERFORMING ORGANIZATION NAME(S) AND ADDRESS(ES)

Edward L. Ginzton Laboratory
Stanford University
Stanford, CA 94305-4088

8. PERFORMING ORGANIZATION REPORT NUMBER

SPO No. 27172

9. SPONSORING / MONITORING AGENCY NAME(S) AND ADDRESS(ES)

AFOSR
801 North Randolph Street, Room 732
Arlington, VA 22203-1977
Dr Howard Schlossberg/NE

10. SPONSOR/MONITOR'S ACRONYM(S)

11. SPONSOR/MONITOR'S REPORT NUMBER(S)

12. DISTRIBUTION / AVAILABILITY STATEMENT

Approved for public release; distribution unlimited.

13. SUPPLEMENTARY NOTES

14. ABSTRACT

This program focused on the development of micro-structured nonlinear optical materials and quasi-phasematched devices based on those materials. The two material systems investigated, periodically-poled ferroelectrics, especially lithium niobate (PPLN), and orientation-patterned GaAs (OP-GaAs), enable nonlinear interactions impossible in conventional nonlinear media. The work included characterization of vapor-transport-equilibrated materials, enhancements in periodic-poling technology, and development of tight bends in proton-exchanged waveguides. After the materials characterization and improvements in process development, we fabricated new devices including OP-GaAs devices for broadband optical parametric generation (OPG) at mid-infrared wavelengths, bulk PPLN devices for soliton amplifiers, and PPLN reverse-proton-exchanged waveguide devices for quasi-group-velocity-matching, telecommunication applications and generation of nearly-transform-limited OPG.

Supplemental MIPR funding from DARPA was used to support and purchase ceramic fabrication equipment for the fabrication of transparent laser host materials, supported primarily under ARO Grant DAAD19-02-1-0184.

15. SUBJECT TERMS

microstructured nonlinear optical materials, quasi-phasematched devices, periodically-poled lithium niobate, orientation-patterned GaAs, stoichiometric lithium tantalate, frequency conversion, non-linear optics

16. SECURITY CLASSIFICATION OF:			17. LIMITATION OF ABSTRACT	18. NUMBER OF PAGES	19a. NAME OF RESPONSIBLE PERSON Martin M. Fejer
a. REPORT	b. ABSTRACT	c. THIS PAGE		29	19b. TELEPHONE NUMBER (include area code) (650) 725-2160

Standard Form 298 (Rev. 8-98)
Prescribed by ANSI Std. Z39.18

1. AFOSR GRANT NUMBER: F49620-02-1-0240

2. PERIOD COVERED BY REPORT: 06/01/2002– 11/14/2006

3. TITLE OF PROPOSAL: Quasi-Phasematched Nonlinear Optics: Materials and Devices

4. LIST OF MANUSCRIPTS SUBMITTED OR PUBLISHED UNDER AFOSR SPONSORSHIP DURING THE COURSE OF THIS PROGRAM:

a. Junqiang Sun; Wei Liu; Jing Tian; Kurz, JR; Fejer, MM,"Multichannel wavelength conversion exploiting cascaded second-order nonlinearity in LiNbO3 waveguides", IEEE Photonics Technology Letters ,No. 12 Vol. 15 pp.1743-45 (December 2003)

b. Jie Huang, J. R. Kurz, Carsten Langrock, A. M. Schober, and M. M. Fejer,"Quasi-group-velocity matching using integrated-optic structures", Optics Letters ,No. 21 Vol. 29 pp.2482-2484 (November 2004)

c. Shang-Da Yang, Andrew M. Weiner, Krishnan R. Parameswaran, Martin M. Fejer,"400-photon-per-pulse ultrashort pulse autocorrelation measurement with aperiodically poled lithium niobate waveguides at 1.55 um", Optics Letters ,No. 17 Vol. 29 pp.2070-2072 (September 2004)

d. K. L. Vodopyanov, O. Levi, P. S. Kuo, T. J. Pinguet, J. S. Harris, M. M. Fejer, B. Gerard, L. Becouarn, E. Lallier,"Optical parametric oscillation in quasi-phase-matched GaAs", Optics Letters ,No. 16 Vol. 29 pp.1912 (August 2004)

e. M. Katz, R.K. Route, D.S. Hum, K.R. Parameswaran, G.D. Miller and M.M. Fejer,"Vapor-transport equilibrated near-stoichiometric lithium tantalate for frequency-conversion applications", Optics Letters ,No. 15 Vol. 29 pp.1775 (August 2004)

f. Jiang, Z.; Seo, D.S.; Yang, S.-D.; Leaird, D.E.; Roussev, R.V.; Langrock, C.; Fejer, M. M; Weiner, A. M.,"Low-Power High-Contrast Coded Waveform Discrimination at 10 GHz Via Nonlinear Processing", Photonics Technology Letters ,No. 7 Vol. 16 pp.1778-1780 (July 2004)

g. Xiuping Xie, Andrew M. Schober, Carsten Langrock, Rostislav V. Roussev, Jonathan R. Kurz, Martin M. Fejer, " Picojoule threshold, picosecond optical parametric generation in reverse proton-exchanged lithium niobate waveguides", JOSA B Vol. 21, No. 7 1397-1402 (July 2004).

h. Rostislav V. Roussev, Carsten Langrock, Jonathan R. Kurz, and M. M. Fejer, "Periodically poled lithium niobate waveguide sum-frequency generator for eff icient single-photon detection at communication wavelengths ", Optics Letters Vol. 29, No. 13 1518-1520 (July 2004).

j. Z. Jiang, D.S. Seo, S.-D. Yang, D.E. Leaird, A.M. Weiner, R.V. Roussev, C. Langrock and M.M. Fejer, "Spectrally coded O-CDMA system with four users at 2.5 Gbit using low power nonlinear processing", Electonics Letters 40, No. 10 (May 2004).

k. Jonathan R. Kurz, Jie Huang, Xiuping Xie, Takashi Saida, and Martin M. Fejer, "Mode multiplexing in optical frequency mixers ", Opt. Lett. 29, No.6 551-553 (March 2004).

l. X. Yu, L. Scaccabarozzi, J. S. Harris, Jr., P. S. Kuo, and M. M. Fejer,"Efficient continuous wave second harmonic generation pumped at 1.55 μm in quasi-phase-matched AlGaAs waveguides", Optics Express, No. 26 Vol. 13 pp.10742-10748 (December 2005)

m. Z. Jiang, D. S. Seo, S. D. Yang, D. E. Leaird, R. V. Roussev, C. Langrock, M. M. Fejer, A. M. Weiner,"Four-user, 2.5-Gb/s, spectrally coded OCDMA system demonstration using low-power nonlinear processing", Journal of Lightwave Technology, No. 1 Vol. 232 pp.143-158 (January 2005)

n. S.-D. Yang, Z. Jiang, A.M. Weiner, K.R. Parameswaran, and M.M. Fejer,"Ultrasensitive chromatic dispersion monitoring for 10 GHz pulse train by quasi-phase-matched LiNbO3 waveguides", Electronics Letters, No. 9 Vol. 41 pp.554-556 (April 2005)

o. A. M. Schober, M. M. Fejer, S. Carrasco, and L. Torner,"Engineering of multi-color spatial solitons with chirped-period quasi-phase-matching gratings in optical parametric amplification", OPTICS LETTERS, No. 15 Vol. 30 pp.1983-1985 (August 2005)

p. A. M. Schober, M. Charbonneau-Lefort, and M. M. Fejer,"Broadband quasi-phase-matched second-harmonic generation of ultrashort optical pulses with spectral angular dispersion",

20071016425

JOURNAL OF THE OPTICAL SOCIETY OF AMERICA B, No. 8 Vol. 22 pp.1699-1713 (August 2005)

q. Carsten Langrock, Eleni Diamanti, Rostislav V. Roussev, Hiroki Takesue, Yoshihisa Yamamoto, and M. M. Fejer,"Highly efficient single-photon detection at communication wavelengths by use of upconversion in reverse-proton-exchanged periodically poled LiNbO3 waveguides", OPTICS LETTERS, No. 13 Vol. 30 pp.1725-1727 (July 2005)

r. Zhi Jiang, Dongsun Seo, Shangda Yang, Daniel E. Leaird, Rostislav V. Roussev, Carsten Langrock, Martin M. Fejer, and Andrew M. Weiner,"Four-User 10-Gb/s Spectrally Phase-Coded O-CDMA System Operating at ~30 fJ/bit", IEEE PHOTONICS TECHNOLOGY LETTERS, No. 3 Vol. 17 pp.705-707 (March 2005)

s. Z. Jiang, D. S. Seo, D. E. Leaird, R. V. Roussev, C. Langrock, M. M. Fejer, and A. M. Weiner,"Reconfigurable All-Optical Code Translation in Spectrally Phase-Coded O-CDMA ", JOURNAL OF LIGHTWAVE TECHNOLOGY, No. 6 Vol. 23 pp.1979-1990 (June 2005)

t. M. Charbonneau-Lefort, M.M. Fejer, and B. Afeyan,"Tandem chirped quasi-phase-matching grating optical parametric amplifier design for simultaneous group delay and gain control", OPTICS LETTERS, No. 30 Vol. 6 pp.634 (March 2005)

u. Jie Huang, X. P. Xie, Carsten Langrock, R. V. Roussev, D. S. Hum, and M. M. Fejer,"Amplitude modulation and apodization of quasi-phase-matched interactions", Optics Letters, No. 5 Vol. 31 pp.604-606 (March 2006)

v. Xiuping Xie, M. M. Fejer,"Two-spatial-mode parametric amplifier in lithium niobate waveguides with asymmetric Y junctions", Optics Letters, No. 6 Vol. 31 pp.799-801 (March 2006)

w. X.P. Xie, J. Huang, and M.M. Fejer,"Narrow-linewidth Near-Degenerate Optical Parametric Generation Achieved with Quasi-group-velocity-matching in Lithium Niobate waveguides", Optics Letters, No. 14 Vol. 31 pp.2190-2192 (July 2006)

x. Xiuping Xie and M. M. Fejer,"Cascaded optical parametric generation in reverse-proton-exchange lithium niobate waveguides", JOSA B, No. 3 Vol. 24 pp.585-591 (March 2007)

y. D. S. Hum, R. K. Route and M. M. Fejer,"Quasi-phase-matched second-harmonic generation of 532 nm radiation in 25-degree-rotated, x-cut, near-stoichiometric, lithium tantalate fabricated by vapor transport equilibration", Optics Letters, No. 8 Vol. 32 pp.961-3 (April 2007)

5. SCIENTIFIC PERSONNEL SUPPORTED BY THIS PROJECT AND DEGREES AWARDED DURING THIS REPORTING PERIOD:

Faculty - M.M. Fejer   Post-Doctoral Scholars – R. Gaume
Senior Staff - R. Route
Students – J. Huang, D. Hum (Ph.D. awarded 2007), P. Kuo , R. Roussev, A. Schober (Ph.D. awarded 2005), J. Wisdom, and X. Xie (Ph.D. awarded 2007)

6. REPORT OF INVENTIONS BY TITLE ONLY:

7. SCIENTIFIC PROGRESS AND ACCOMPLISHMENTS: See Final Technical Report

8. TECHNOLOGY TRANSFER:

This program explored micro-structured nonlinear optical materials and quasi-phasematched (QPM) nonlinear devices based on them. Technology developed under this and predecessor programs let to numerous collaborations with industry and academic institutions. Most recently we have collaborated with LLNL, MIT Lincoln Labs, CeLight, Sony, UCSC (Center for Adaptive Optics), Purdue, USC, U. New Mexico.

9. CORRESPONDENCE ADDRESS:

Martin M. Fejer, P.I.
Ginzton Laboratory, Mail Code 4088   (tel) 650-725-2160
Stanford University   (fax) 650-723-2666
Stanford, CA 94305-4088   fejer@stanford.edu

SF 298 Continuation Sheet
Final Technical Report
AFOSR GRANT: F49620-02-1-0240

Table of Contents

REPORT DOCUMENTATION, Cont. (SF298)

Final Technical Report
on
F49620-02-1-0240
Award: Quasi-Phasematched Nonlinear Optics: Materials and Devices
Award dates: 01-Jun-2002 through 14-Nov-2006
Award amount: $600,000

Supplemental award: Ceramic Laser Development
Supplemental award dates: 18-Jan-2005 through 14-Nov-2005
Supplemental award amount: $300,000

Report period: 01-Jun-2002 through 14-Nov-2006

M. M. Fejer, P.I.
Stanford University

I. Introduction

During the three years of support that ended 31-May-2005, we investigated microstructured ferroelectric and semiconductor nonlinear materials and the bulk and waveguide nonlinear interactions that they enable. Through the intrinsically large nonlinearity of these materials, and the degrees of engineering freedom afforded by the quasi-phasematching (QPM) techniques, it has been possible to demonstrate a variety of novel devices. Among these are optical parametric oscillators (OPOs) tunable from 2.4 – 11 μm, optical parametric generators (OPGs) producing continua extending from 4.8 – 8.5 μm, chirped-grating optical parametric amplifiers (OPAs) enabling efficient launching of spatial solitons, and a waveguide OPG device with a threshold below 200 pJ. Ultrafast concepts developed include tandem-QPM-grating OPAs with constant group delay over very-wide spectral bandwidths, and noncollinear QPM SHG interactions allowing generation of transform-limited output in crystals much longer than the group-velocity-mismatch (GVM) length.

These devices are enabled by progress in microstructured materials. Orientation-patterned GaAs (OP-GaAs), a thick-film semiconductor nonlinear material with periodic twins controlled by a lithographically patterned template, extends QPM techniques into the mid-IR beyond the multi-phonon absorption edge that limits oxide ferroelectrics. The vapor-transport-equilibration (VTE) process allows convenient production of stoichiometric ferroelectrics from readily available congruent-composition substrates, including stoichiometric lithium tantalate (SLT) and stoichiometric magnesium-doped lithium niobate (SMg:LN). Both these materials show negligible room-temperature photorefractive and photochromic effects, which have limited applicability of congruent-composition crystals for visible-light applications. An indication of the improved performance of these materials was the demonstration of 5-W-average-power second harmonic generation (SHG) of 532-nm generation for 1000 hours at room temperature in a PPSLT crystal.

This work was completed as of 14-Nov-2005, and the results on that component of the program were reported in the 2005 annual technical report. The work is recapped here for completeness. It has subsequently been continued under AFOSR Grant FA9550-05-1-0180 and FA9550-07-1-0100.

The supplemental modification resulted from a DARPA Seedling award which was funded via a MIPR through AFOSR. The supplemental modification supports ARO Grant DAAD19-02-1-0184 under PI – Robert L. Byer with title "High Average Power Diode-Pumped Solid-State Lasers: Power

2

Scaling with High Spectral and Spatial Coherence". The supplemental modification was for a critical set of capital equipment to fabricate transparent ceramic devices and explore new transparent ceramic materials. The initial devices proposed were planar waveguide structures based on Nd:YAG and integrated passively Q-switched Nd:YAG gain media. The supplemental modification included funds for capital equipment as well as salary support for a post-doctoral affiliate. The supplemental award amount was not yet expended by 14-Nov-2005, and a no-cost extension was requested to extend the program through 15-Nov-2006. Work completed under the Supplemental Modification is reported here, as well as under DAAD19-02-1-0184.

II. Recap of Results on Quasi-Phasematched Nonlinear Optics: Materials and Devices (Completed as of 14-Nov-2005 and reported in the 2005 annual technical report)

A. Schober, X-P Xie, J. Huang, D. Hum, R. Roussev,

II.1 Materials

Our materials work over the past three years has made progress in four broad areas: synthesis and characterization of stoichiometric lithium niobate and tantalate with improved ferroelectric and optical properties compared to conventional congruently melting crystals; improved periodic-poling technology in conventional ferroelectrics; orientation-patterned III-V semiconductors as analogues to PPLN for mid-IR QPM; and improved waveguide fabrication in ferroelectric materials. These projects are reviewed briefly here, as they set the stage for several of the proposed materials and device projects.

II.1.1 Stoichiometric Ferroelectrics

Stoichiometric lithium tantalate
Our work to date has established that the vapor-transport equilibration (VTE) method is capable of producing crystals of both LN and LT that are closer to stoichiometry than those produced by other means. In stoichiometric lithium tantalate (SLT), the concomitant reduction in stoichiometric point defect density (by approximately two orders of magnitude) has two key effects: the photoconductivity is increased in proportion to the reduction in defect density (presumably through an increase in the carrier lifetime) and the coercive field for domain reversal is also reduced by approximately two orders of magnitude (as low as 60 V/mm compared to 20 kV/mm in congruent crystals). The high photoconductivity without increase in photogalvanic current results in no measurable room-temperature photorefractive damage, and easier poling of thicker wafers as well as rotated-cut wafers without dielectric breakdown or fracture.

To test for long-term aging effects, periodically-poled stoichiometric lithium tantalate (PPSLT) was used to generate 5-W average power of 532 nm light by SHG with a 100-kHz repetition Q-switched pump laser. This experiment was then monitored for over 1000 hours of continuous operation, as shown in Figure 1.[1] The conversion efficiency in PPSLT showed no degradation over the life of the experiment. Thus, at these experimental intensities (up to 2 MW/cm²), photorefractive and photochromic effects do not limit the utility of this material. Investigations at higher intensities and higher average powers will be necessary to assess the limiting issues in this material.
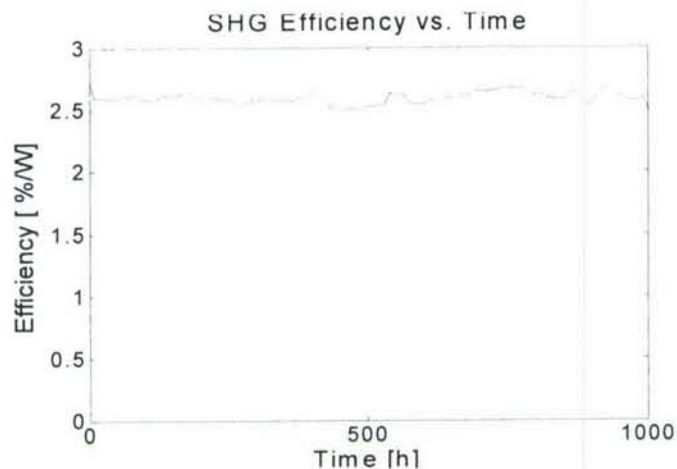
Figure 1. SHG efficiency in PPSLT was measured at room temperature over 1000 hours and shows no degradation at 5-W average power. Photorefractive and photochromic effects that limit conventional congruent-composition crystals do not affect the performance of the PPSLT crystal.

Stoichiometric lithium niobate

A related set of questions apply to stoichiometric lithium niobate (SLN). Compared to SLT, SLN has higher nonlinear coefficient allowing a factor of two improvement in conversion efficiency in bulk crystals. In addition, APE and RPE waveguides in SLN should provide tighter confinement of the light and higher intensity at the same power level, increasing conversion efficiency of waveguides further compared to SLT. Thus SLN is more attractive than SLT for lower power applications. However, so far no pure SLN has shown the photorefractive damage resistance that is commonly found in SLT.

VTE on CLN was extensively studied over a decade ago[2]. As in LT, the process has been demonstrated to result in uniform crystals after sufficient diffusion time, although the apparent self-termination happens farther from the stoichiometric composition. The coercive field of VTE SLN reported to date has been ~2 kV/mm[3], suggesting a composition which is 10 times closer to stoichiometric compared to CLN, but still 0.16 % deficient in Li. We were able to obtain VTE SLN with a coercive field of ~1 kV/mm, twice as close to stoichiometric as in earlier reports. Yet, the photorefractive sensitivity of SLN was not reduced compared to CLN. According to the model for the photorefractive damage that successfully explains the results in VTE SLT, we would expect that carrier lifetime in our VTE SLN to be ~20 times longer than in CLN, leading to 20 times higher photoconductivity and correspondingly smaller sensitivity to PRE, none of which were observed experimentally. Clearly, a more complex model needs to be developed in order to explain PRE in VTE SLN.

Given the otherwise markedly similar structural and optical properties of these crystals, the difference is puzzling. Perhaps the most likely explanation is that the phase boundary for SLN lies slightly on the lithium-poor side of stoichiometry, so that a non-negligible number of anti-site Nb remain after the VTE process. The much greater photorefractive damage resistance of stoichiometric LN crystals with even small amounts of Mg-doping[4] is consistent with this interpretation. Vapor transport equilibration of congruent lithium niobate (CLN) grown by Crystal Tech with various low Mg concentrations was carried out. Tests showed that PRE was eliminated in crystals saturated with lithium, for [Mg]>0.3%. Some difficulties remain in indiffusion of Li under conditions that simultaneously maintain crystal quality and proceed in less than a couple of hundred hours. Further work is required to find suitable conditions for producing high quality VTE Mg:SLN, in particular that VTE times required to reach PRE-resistant compositions, especially in 0.3%Mg-doped crystals, are longer than is convenient, and some changes in coloration often occur during the VTE process.

4

Nonlinear susceptibility of congruent and stoichiometric ferroelectrics

Literature reports asserted that stoichiometric ferroelectrics show a 30% larger nonlinear susceptibility than the corresponding congruent-composition crystals. As such a result would have important implications for many device applications, we carried out Maker fringe measurements of SHG at 1.06 μm on several stoichiometric materials, normalized to congruent LN samples. Within 5%, we found that d_{33} was affected by neither VTE nor simultaneous VTE and Mg doping. The table below summarizes the experimental results, with the measured d_{33} normalized to that of congruent LN, contradicting the prior literature results.

Material	Normalized d_{33}
Congruent LN	100%
200h VTE LN	100%
400h VTE LN	101%
1% Mg:LN	99%
Congruent LT	64%
SLT	66%
Mg:SLT	67%

Table 1. Relative nonlinear susceptibilities measured for various congruent and stoichiometric ferroelectrics.

II.1.2 Periodic Poling Technology

The extremely low coercive fields characteristic of stoichiometric crystals suggested that it might be possible to pole plates of orientations other than the standard z-axis, with applications, for example, to face-pumped nonlinear devices (section III.2.1). A plate cut at 45° to the z-axis would have an effective nonlinear coefficient for reasonable angles of incidence that is within $1/\sqrt{2}$ of that for propagation normal to z, and similarly the projection of the poling field on the z-axis would be $1/\sqrt{2}$ of the total field, as shown in Figure 2.

Figure 2. Off-normal poling of stoichiometric crystal. High energy of charged domain wall leads to propagation parallel to the ferroelectric axis.

Preliminary exploration of rotated CLN plates indicated that the domains would still grow parallel to the z-axis, but the high poling fields precluded systematic exploration of this option. The two-orders of magnitude lower poling fields required for SLT and SLN lift this constraint, so we investigated this possibility in SLT wafers. Commercially available, surface acoustic wave substrates were treated with the VTE process to lower the coercive field, allowing periodic poling before piezoelectric strain caused mechanical failure, as was the case in poling of rotated cuts of congruent materials. The samples revealed that domain patterning is possible in such materials, as shown in Figure 3.. The grating produced had a period of 41 μm and preliminary experiments showed the expected SHG in this configuration.[5]

Further investigations to reduce the poling period, and increase the wafer thickness and poling angle are required for this material to be used for practical face-pumped devices. Experimental measurements of the laser-induced surface damage threshold are required to probe the limits of this material for scaling to higher and higher average and peak powers. Upon completion of these studies, face-pumped topologies for efficient SHG of nearly arbitrarily high energy (over 100 J) pulses.
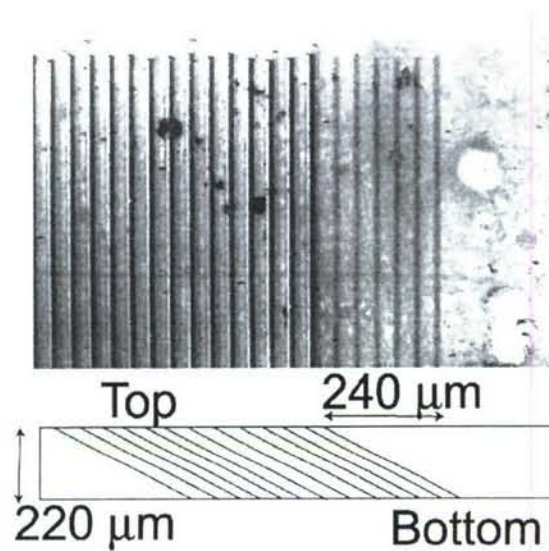
Figure 3. Periodic poling of 42° rotated Y-cut SLT. Scattering from the back face reveals that the domains are slanted 48° from the surface normal

II.1.3 Orientation-Patterned GaAs

Means for quasi-phasematching in the III-V semiconductors are attractive, as these materials have large nonlinear susceptibilities ($d_{14}(GaAs) = 5$ x $d_{33}(LiNbO_3)$), broad IR transparency (to >12 µm in GaAs), and high thermal conductivities (~ 10 x $LiNbO_3$) that reduce the temperature rise resulting from absorbed optical power. Since they have a $\bar{4}$ axis in the (100) direction, 90° twins around this axis invert the crystal structure, and so change the sign of the nonlinear susceptibility as is required for QPM. We have developed methods for lithographically patterning a substrate, to create a template that controls the orientation of subsequently grown films. This orientation-patterned GaAs (OP-GaAs) can be grown in thin-film form by MBE, or in thick films by hydride vapor-phase epitaxy (HVPE).[6] This material has exceptional properties for mid-IR nonlinear devices, simultaneously providing all the well-known advantages of QPM techniques while moving the multi-phonon absorption edge from the 4.5 µm limit in PPLN to > 12 µm in Op-GaAs, and providing a figure of merit (d^2/n^2) for focused nonlinear interactions 10 x larger than that of PPLN at the same wavelength, due to the larger nonlinear susceptibility of OP-GaAs (~ 100 pm/V).[7]

This material is truly a mid-IR analogue of PPLN, and has opened this spectral range to the same range of techniques, as discussed here. A number of other programs contribute support to the further development of this material (and analogues like OP-GaP). It has been used in this program to extend the range of the techniques proposed, and as a material supporting the ultrafast portions of the program with a uniquely broad-band performance (> octave bandwidth) as a mid-IR parametric amplifier.

II.1.4 Waveguide Fabrication

Highly efficient waveguide frequency mixers are useful both for frequency conversion applications as well as for classical and quantum optical signal processing devices, and ultrafast pulse characterization. We have further developed the reverse-proton exchange waveguide process in congruent lithium niobate, with losses as low as 0.1 dB/cm in devices with confinement optimized for high mixing efficiency. Tight waveguide bends, based on tight optical confinement and selective etching to produce depressed claddings to reduce radiation loss are also under development.

II.2 Devices

We have had exciting results in a number of device applications of microstructured nonlinear materials, in both bulk and waveguide configurations. Mid-IR devices based on OP-GaAs as an analogue of PPLN with extended IR transparency has yielded both OPO and OPG devices with unprecedented performance. Ultrafast devices include novel concepts like quasi-group-velocity matching, and several new types of wide-bandwidth parametric amplifiers.

II.2.1 Mid-IR Devices

Optical parametric oscillators (OPO)

We demonstrated the first optical parametric oscillator (OPO) based on orientation-patterned GaAs.[8] The experimental setup for the GaAs OPO is shown in Figure 4. The OP-GaAs sample was 0.5-mm thick (along [001]), 5-mm wide (along [1 $\overline{1}$0]) and 11-mm long (along [110], the optical beam propagation direction), and the optical faces were AR-coated (R<2% per facet) for $\lambda = 1.5 - 3$ μm. The optical losses inside the sample were estimated to be less than 0.04 cm^{-1} at 1.55 μm. The inset in Figure 4 shows a stain-etched cross-section of our OP-GaAs sample, taken with a Nomarski microscope.
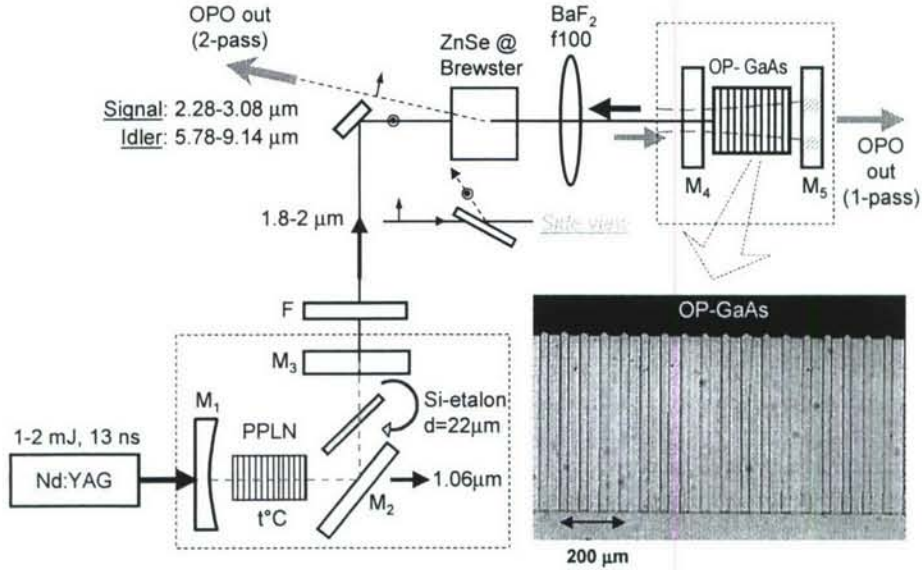

Figure 4. Schematic of the OP-GaAs OPO. In the case of a double-pass OPO setup, mirror M_5 is metallic and the backward OPO output is reflected by a ZnSe Brewster plate; in the case of a single-pass setup, the forward output goes through dielectric mirror M_5. Inset: Stain-etched cross-section of a 500-μm-thick OP-GaAs sample.

For the available 61.2-μm-QPM-period OP-GaAs sample, we used a PPLN OPO to produce the required 1.8-2 μm pump radiation. The bandwidth of the signal output of the PPLN OPO was 5 cm^{-1}, which is within the pump-acceptance bandwidth of the OP-GaAs (approximately 6 cm^{-1}).

The lowest threshold and the highest output were obtained in a two-pass arrangement in the GaAs OPO. The pump pulses (0-200 μJ, 6 ns, M^2=2.3), polarized along the [001] axis of the OP-GaAs, were focused into the sample to a 1/e^2 intensity radius w_0 = 180 μm. The pump threshold of the OP-GaAs OPO was as low as 16 μJ (fluence 0.03 J/cm^2) which is consistent with the predictions of our numerical model which gives 13 μJ.

By tuning the pump wavelength between 1.74 and 2.05 μm the GaAs OPO yielded continuously tunable output (measured with a grating monochromator) from 2.1 to 3.1 μm (signal) and 5.8 to 11.1 μm (idler), as shown in Figure 5. This tuning range was limited entirely by the reflectivity range of our dielectric OPO mirrors: with the proper mirror set, continuous 1.8-17 μm OPO tuning can be achieved with this sample by tuning the pump from 1.6 to 2.07 μm.
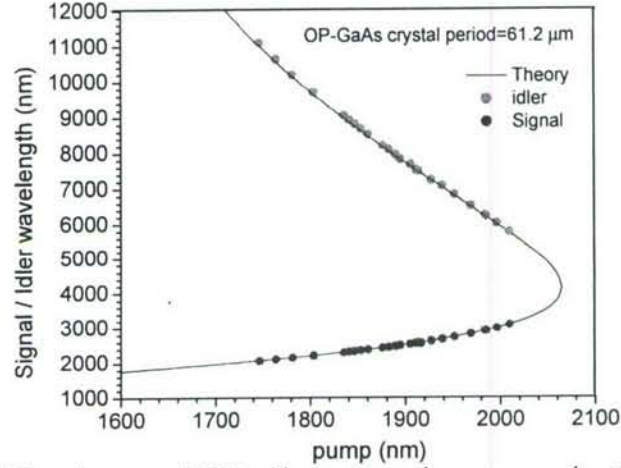

Figure 5. OP-GaAs OPO tuning curve (20°C) with respect to the pump wavelength. Solid line – calculated.

We also investigated the dependence on pump polarization. We observed an increase in the output, as expect, by pumping along [111]. We demonstrated OPO operation with pump polarized along [001] as well as along [110], which suggests the interesting possibility of using either a circularly polarized or even unpolarized beam to pump the OP-GaAs-based OPO.

Ultra-broadband optical parametric generation
We recently demonstrated an optical parametric generator based on OP-GaAs.[9] The OP-GaAs was pumped at λ≈3.3μm wavelength, which is a special point for GaAs since at the OPA-degenerate wavelength, near 6.6 μm, the group velocity dispersion of GaAs vanishes, resulting in an extremely broad (up to an octave or more) parametric gain acceptance bandwidth (see Figure 6).
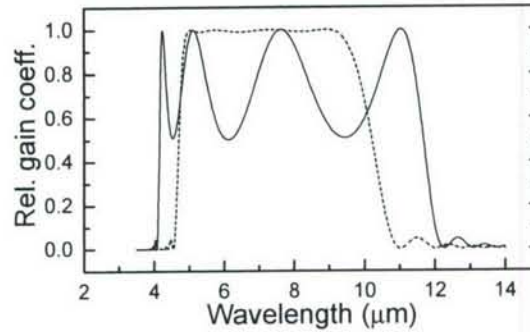
Figure 6. Relative gain coefficient for QPM interactions for 10-mm long GaAs gratings where the period Λ has been optimized for large bandwidth. The solid line represents a pump wavelength of 3.059 μm at room temperature, which results in a bandwidth from 4.1 to 11.7 μm with relative gain variations of 50%. The dashed line represents a pump wavelength of 3.217 μm at a temperature of 20°C, which results in less than 1% gain variation from 4.9 to 9.2 μm.
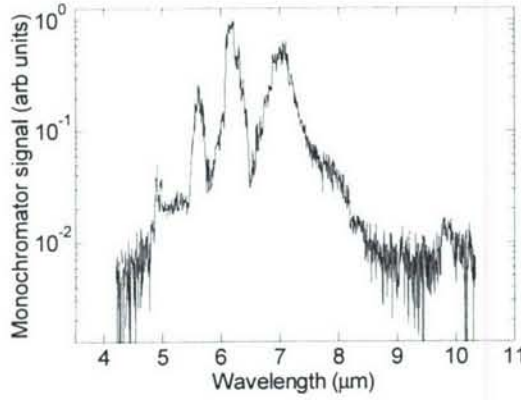
8

Figure 7. OPG spectrum demonstrating output between 4.8 and 8.5-μm wavelength. Dips are due to water absorption and non-uniform monochromator response.

Tunable mid-IR pump pulses for our optical parametric generation experiment were produced with a Spectra-Physics OPA-800 system (λ=3.1-3.3μm wavelength, 1 ps, ~0.5 μJ). Three OP-GaAs samples labeled D, E, and A, with QPM periods 154.2, 166.6 and 168 μm, respectively. The group velocity walk-off length between pump and degenerate signal-idler is ~1 cm for 1 ps pulses, so the interaction length for all three samples is limited to about 1 cm. The samples were AR-coated with R<0.5% at signal and R<5% at the idler, and R=8-15% per surface for the pump.

The pump was focused to a 65-μm-radius spot in the OP-GaAs. The OPG threshold was measured to be approximately 100 nJ for all samples, corresponding to 1.5-GW/cm² intensity. The OPG spectra were measured with a ¼-meter grating monochromator. Figure 7 shows the OPG output spectrum for sample E with a 300-nJ, 3.27-μm pump. A spectrum spanning from 4.8 to 8.5 μm (20dB down from the peak at 6.3 μm) was generated. Dips in the middle of the measured spectrum are due to (i) water absorption (the apparatus was not purged) and (ii) non-uniformity of the efficiency of the grating spectrometer.

II.2.2 Ultrafast Optical Devices

The engineering degrees of freedom available in QPM devices allow lifting of many of the constraints that have conventionally limited efficiency-bandwidth tradeoffs in ultrafast nonlinear optical interactions. We have investigated a number of these opportunities in the past.[10,11,12,13,14]. In this section we discuss two methods for dealing with bandwidth limitations in nonlinear interactions, noncollinear interactions in QPM media, and quasi-group-velocity matching in waveguide interactions. Section II.2.3 discusses wideband amplifier configurations.

The bandwidth of collinear second-harmonic generation is limited by the mismatch in group velocity between the pump wave and the generated harmonic. This bandwidth can spoil the short duration of ultrafast pump pulses in the process of second harmonic generation if the interaction length L is longer than the characteristic walk-off length $L_{\overline{x}}$. A typical solution is to use a crystal that is shorter than the walk-off length. The maximum conversion efficiency possible in such a collinear interaction limited by group velocity mismatch is achieved by confocal focusing into a crystal that is approximately one walk-off length long. The typical walk-off for SHG in periodically poled materials is between 0.2 and 1.0 ps/mm so that for sub-picosecond pulses, the interaction length is limited to crystals of order 1 mm or shorter. Confocal focusing in short crystals for maximum efficiency results in high peak intensity which can result in appreciable multiphoton absorption or optical damage.

One way to circumvent the limitations of group-velocity mismatch, shown in Figure 8, is to use spectral angular dispersion in a critical phase-matching geometry. Since the different frequency
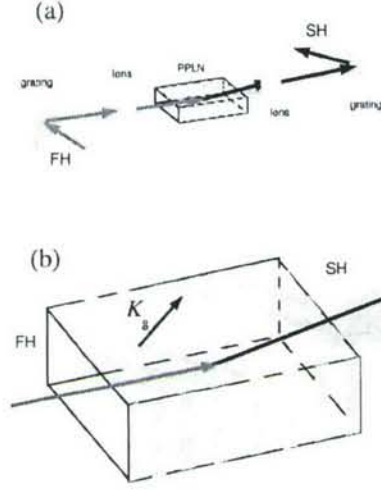
9

(a)

(b)

Figure 8. Schematic diagram of PPLN experiment with spectral angular dispersion. Angular dispersion imposed by a diffraction grating provides built-in angular tuning of the SHG interaction enabling simultaneous phase-matching of all frequency components of an ultrashort pulse. A non-collinear geometry is necessary in QPM materials to provide the critical phase matching necessary for linear tuning of the phase-matching angle with wavelength.

components of a short optical pulse will phase-match at different incident angles in a nonlinear crystal, using angular dispersion can program angle tuning into the first-harmonic pump field. In this manner, the limitations of frequency-dependent phase matching seen through group-velocity mismatch can be managed by properly matching the angular dispersion of the first-harmonic field to the angular dispersion required to maintain phase-matching.[15]

We demonstrated this technique in a 1-cm-length PPLN crystal using 150 fs pulses at a first-harmonic wavelength of 1550 nm for which the group-velocity mismatch is 0.3 ps/mm. The results in Figure 9 show that even though the interaction length is much longer than the walk-off length, the full bandwidth of the FH pulse is still converted. For comparison we also show the bandwidth and autocorrelation for the conventional collinear interaction which is severely limited by group-velocity mismatch. We also developed rigorous theoretical analysis of SHG with spectral angular dispersion that accurately predicts the conversion efficiency. This analysis also shows that the maximum conversion efficiency under optimum focusing and phase-matching conditions is approximately equal to the maximum efficiency under collinear conditions in a short crystal, but demonstrates a clear advantage in achieving this efficiency at a peak intensity that is approximately L_g^2/L^2 below the peak intensity for the collinear interaction. The results of this experiment as well as the theoretical analysis were submitted to the Journal of the Optical Society of America B in October 2004, and presented at Photonics West 2005. Quasi-Group-Velocity Matching
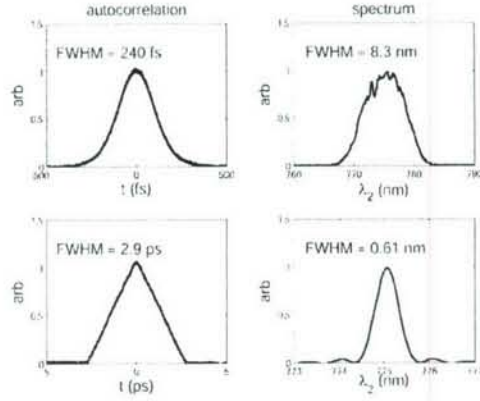
Figure 9. Results of broadband SHG with spectral angular dispersion in PPLN. Autocorrelation (left) and spectrum (right) of SHG with spectral angular dispersion (top) is compared with collinear SHG in an identical length crystal in the presence of group-velocity walkoff (bottom). With spectral angular dispersion, the phase matching bandwidth is nearly 14 times broader than the bandwidth of collinear SHG in a crystal of the same length.

A limitation on nonlinear interactions between ultrafast pulses is the difference in group velocities between the interacting fields. This group velocity mismatch (GVM) leads to temporal walkoff, limiting the useful interaction length to the distance over which the pulse envelopes walk off each other. For PPLN in the vicinity of 1.5 um fundamental wavelength, the maximum interaction length is limited by group-velocity walkoff to an interaction length of 3 mm. Since the efficiency scales with the square of the interaction length, this limitation on the efficiency is significant – the high efficiency of ultrafast QPM devices stems from the large nonlinear coefficient making up for the rather strong walkoff effects. Means to ameliorate the walkoff effect would enable a further quadratic increase in efficiency, with potential for operation at the femtojoule level.

With this motivation, we have been exploring a concept we have called "quasi-group-velocity matching" (QGVM) in which a periodic time delay is inserted for one of the interacting waves to reset the timing of its envelope compared to that of the slower wave, e.g. the 1.5 μm signal interacting with a 780 nm pump. The device is very much analogous to the use of periodic sign changes in $\chi^{(2)}$ to compensate for phase-velocity mismatch, hence the term QGVM. The waveguide components described in section II.1.4 enable the fabrication of the required structures; a first pass at this device showed promising results. We anticipate that successful operation would occur after one or two more design iterations.
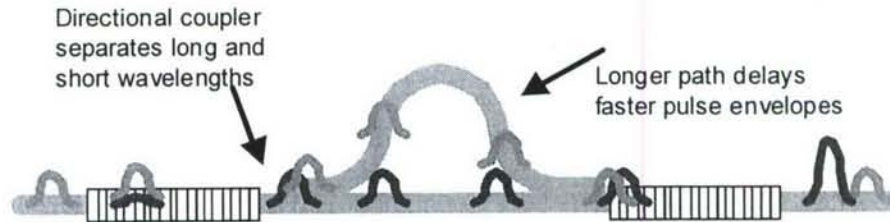
Figure 10. Quasi-group-velocity matching (QGVM). The walkoff of the envelopes of the interacting waves is reset by inserting a periodic time delay. The efficiency increases as N^2 for N such sections in the device.

We have demonstrated a two-stage device in APE lithium niobate waveguide.[16] Two approximately 150-fs-long pulses generated 6 ps apart by SHG in two QPM gratings were re-synchronized by the fixed delay line. (Figure 10) The accuracy of GVM compensation, measured by the mismatch of

pulse envelopes at output, was better than 80 fs. The relative phase of the two pulses was fine controlled by temperature tuning to ensure maximum SHG efficiency, Figure 11. This temperature tuning approach lifts the requirement for precise positioning of QPM gratings, and makes the fabrication much easier. The temperature-tuning period, according to design as well as verified in experiment, was 8° C, a practically good number for easy control and stable operation of the device. The QGVM technique, which can be iterated to more than two segments, enables optical frequency mixers of higher efficiency-bandwidth product than would be possible in a single grating. It is now being used in ultrafast OPG devices. In future work, multi-section devices, fundamental limitations imposed on them by GVD, and practical limitations due to finite bend radii will be investigated.
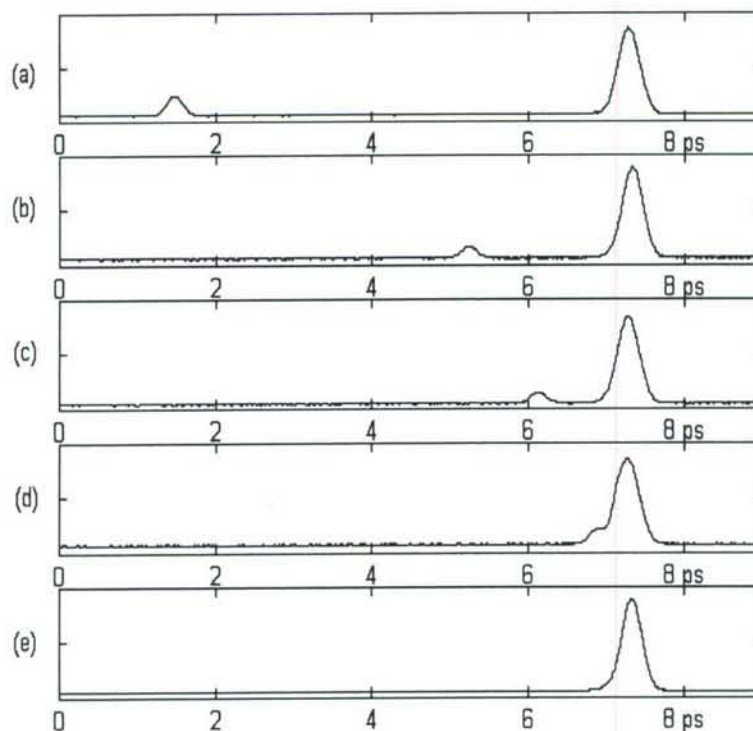

Figure 11. Cross-correlation traces of a reference device (a) and four GVM compensation devices with different amount of delay (b)-(e).

Ultralow-Threshold Waveguide Optical Parametric Generation

Optical parametric generation (OPG), is a very simple method for generating tunable radiation, especially ultrafast pulses, essentially by amplifying vacuum noise to macroscopic powers in high-gain ($\sim 10^{10}$) parametric amplifiers. Two limitations on the method have been that it requires rather high energy pump pulses in conventional materials, and that without additional complexity generally generates pulses that are far from transform limited.[17] QPM materials have removed one of these limitations, with enough gain to reach OPG threshold with 25 nJ in bulk PPLN,[18] and < 1 nJ in a PPLN waveguide.[19] The other issue is that absent special dispersion conditions, simple OPG devices produce pulses whose spectrum is substantially broader than the transform limit. Several of the tools developed in our prior work are useful for addressing these issues.

A PPLN waveguide parametric generator with a threshold of only 200 pJ (vs the microjoule values typical in bulk media) for 1.8 ps pulses was demonstrated. Through a cascade of OPG and sum

12

frequency generation (SFG), transform limited pulses were generated. This work was recently published in Ref. 20.

In the experiments with 40-mm-long quasi-phase-matching (QPM) gratings in reverse-proton-exchanged waveguides, a pump pulse with FWHM length of 1.8 ps at 769.6 nm yielded an OPG threshold of 200 pJ. The quasi-phase-matched OPG demonstrated up to 33% saturated photon conversion efficiency (internal) with 1 nJ pump pulses. The single-pass OPG was tunable from 1.15 μm to 2.3 μm for pump wavelengths between 770 nm and 789.5 nm.

When the generated outputs occur simultaneously with a cascaded SFG process, they can be near transform-limited, even in the presence of significant group velocity mismatch. As compared to the conventional OPG where the cascade process is absent, we call this process cascaded OPG. Here because the sum frequency has a higher group index than the pump, the portion of the signal (or idler) from the back conversion of SFG has an apparent effective group velocity slower than the pump. Therefore, the group index of the pump is between those of the signal and idler and the signal output is transform-limited.

The dynamics of the cascaded process is revealed by the numerical simulations: if we fix the grating length and increase the pump power, conventional OPG will reach threshold first, with dips appearing at wavelengths where the SFG QPM condition are satisfied; further increasing the pump power, the cascaded OPG will reach its threshold and grow up exponentially faster than the conventional OPG products, because of the group velocity matching.

This process was clear in the experimental results for an 18-mm-long QPM grating, shown in Figure 12. The shape and length of the pulse was measured with the cross-correlation between the signal and a small portion split from the pump. The cascaded product emerges as a separate peak both in the time domain and the frequency domain. If we consider only the cascaded product component, the TBP of the generated signal was 0.51 with a pulse length of 1.9 ps and a bandwidth of 1.4 nm. The conventional OPG product had a TBP of 4.4. Transform-limited TBP for the supposed secant pulse shape is 0.315. By making use of the cascaded process, we have therefore generated a signal with much reduced TBP. We also demonstrated that engineering multi-component QPM grating allows selection of the signal wavelength where the cascaded process occurs.
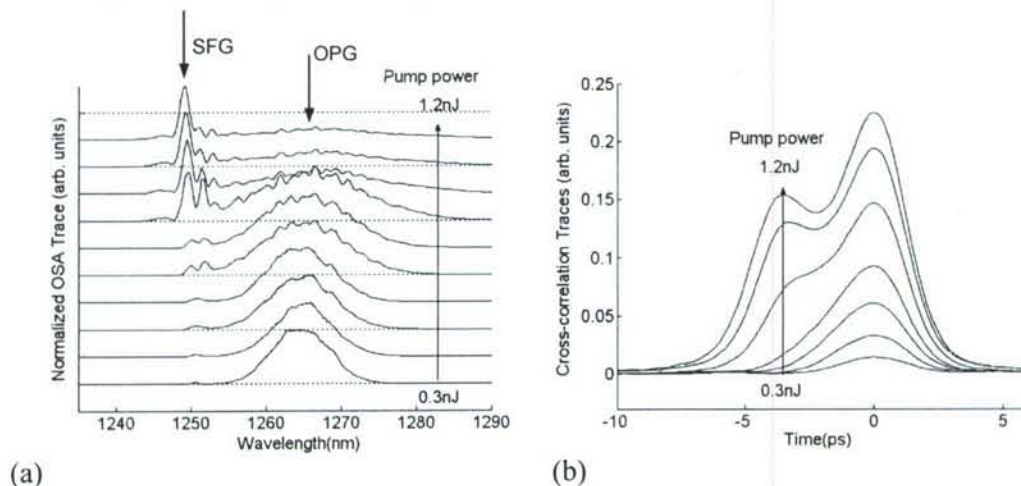

Figure 12 (a) Optical spectrum analyzer traces (b) Cross-correlation traces for the signal from OPG. Both cover the same pump power range from 0.3 nJ to 1.2 nJ. Note the shift of spectrum from conventional-OPG to cascaded output with increasing pump energy. Cross-correlation traces also show both products.

II.2.3 Novel Amplifiers

The high single-pass gains presented by OPAs offer an alternative to regenerative laser amplifiers for ultrafast pulse amplification. The broad bandwidths available in QPM parametric amplifiers, as well as their readily tailored spectral amplitude and phase responses make possible several useful optical power amplification schemes. These properties make PCPA (parametric chirped pulse amplifiers) attractive[21] compared to conventional chirped pulse laser amplifiers. Further adding waveguide interactions to the mix, one has the possibility of large parametric gains with milliwatt peak powers or picojoule pulse energies, enabling other types of interactions.

We have analyzed the effects of chirped QPM gratings on gain and bandwidths of OPAs, and developed both simple physical pictures and numerical methods to analyze these structures. We have had an Optics Letter accepted that describes this analysis, and also examines a new design, a tandem grating in which the group velocity dispersion can be completely cancelled, even over the bandwidth of a 5 fs pulse, while providing 60 dB parametric gain. These amplifiers are also applicable as the gain elements in OPOs. The use of spatial solitons in a parametric amplifier gives another degree of freedom in control over the spatial distribution of the generated radiation.
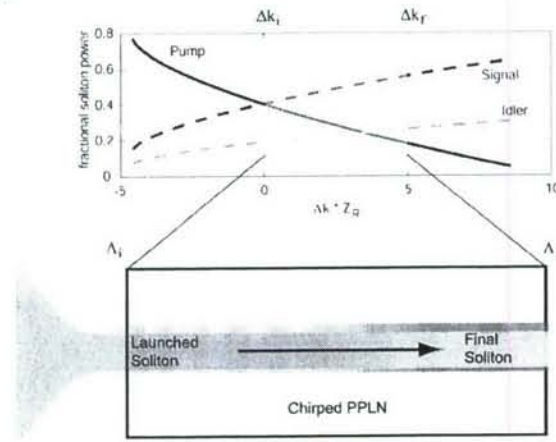
Soliton Parametric Amplifier

Figure 13. Schematic diagram of soliton shaping experiment. The graph shows the soliton fractional power versus the wavevector mismatch Δk in units of the diffraction length $Z_R = k_3\,r_0^2$ where k_3 is the pump wavevector and r_0 is the soliton waist for the pump wave at $\Delta k = 0$. In our chirped grating experiment, the initial wavevector mismatch is zero ($\Delta k_i = 0$) and the final wavevector mismatch is chosen according to the desired output state. The launched soliton experiences a transformation that follows the local soliton state determined by the local wavevector mismatch along the length of a chirped PPLN grating. The fractional soliton power (defined as the power in each component wave divided by the total power) carried in each component of the output soliton is determined by the final value of the wavevector mismatch Δk_f.

Parametric amplifiers have thus far demonstrated advantages over their laser counterparts in producing high single-pass gain over large amplification bandwidths, but have also demonstrated significant difficulty in the efficient extraction of energy over real pulse envelopes. The non-uniform spatial gain profile due to the transverse intensity profile of the pump beam has very large gain in the center of the beam, and significantly less gain in the wings, even where there remains a significant amount of optical power. Such a nonuniform gain distribution complicates efficient extraction of the energy in the pump beam. One potential solution is the use of nonlinearity-induced waveguides, or spatial solitary waves. In this manner, analogous to the traditional optical guided waves, parametric spatial solitary waves travel in specific "nonlinear guided modes" that exist through coupling between pump, signal, and idler waves. In such a coupled wave, all spatial parts of the signal sample all spatial

14

parts of the pump so that spatial non-uniformities in the parametric gain are averaged over the beam. Early chirped-pulse OPA experiments benefited from the spontaneous appearance of this effect to enable photon efficiencies of 30– 40%.[22] Aperiodic QPM gratings offer the possibility of pushing to photon efficiencies in excess of 90%. For a given total power, the ratio of pump power (and, correspondingly, signal and idler power) in the soliton is determined uniquely by the phase mismatch. A chirped QPM grating thus provides the means to adiabatically convert from a soliton which is composed mostly of pump at the input to the device, to an output that is composed mostly of signal and idler. This behavior is weakly dependent on the peak power and the local frequency, enabling its implementation in parametric chirped pulse amplification (PCPA) schemes. Numerical simulations have demonstrated the possibility to deliver photon conversion efficiency approaching 90% in a nearly diffraction-limited output beam with devices available through current QPM technology.[23]

Quasi-phase-matching (QPM) provides unique capability for engineering the amplitude and phase of the nonlinear response in a given material. As shown in Figure 13, the properties of multicolor stationary states depend on the wavevector mismatch. Through the use of a chirped QPM grating, we demonstrate the transformation from a launched soliton state to a different soliton state through the use of a chirped QPM grating in a seeded optical parametric amplifier. In addition to providing the capability of producing soliton states which are difficult to launch in a uniform nonlinear material, this behavior may prove useful for improving the efficiency and/or mode quality in an optical parametric amplifier.[23,24]

We carried out experiments in chirped QPM gratings with variety of chirp rates, using a Q-switched microchip laser producing 0.5-ns 1.06-μm pump pulses, and a CW 1.5-μm seed. Figure 14 shows experimental and theoretical data for the fraction of the soliton energy in pump, signal and idler waves as a function of the final wave-vector mismatch in the chirped QPM gratings. We see good agreement of the relative powers, and can generate solitons with only a small fraction of the energy remaining in the pump at the output. The launching efficiency is lower than theoretical for an ideal gaussian pump beam, presumably reflecting the $M^2 > 1.5$ of the pump beam we used. With an incident pump-pulse energies of 23-25 μJ, we observed a soliton energy between 4 and 6 μJ resulting in a launch efficiency between 16% and 23% near the soliton threshold for $\Delta k = 0$. We compare our experimental data with beam propagation simulations that yield the same total soliton power (i.e. the simulation uses a lower incident power than the experiment, launching 8 μJ).
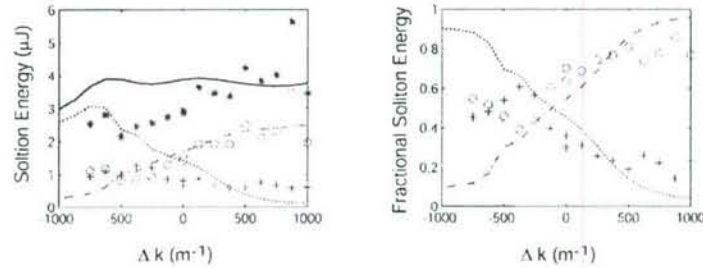

Figure 14. Properties of tailored soliton states. On the left is the energy in the quadratic soliton of the pump (crosses = experiment, dotted line = simulation), signal (circles = experiment, dashed line = simulation) and total (asterisk = experiment, solid line = simulation) in chirped gratings versus the final wavevector mismatch. The initial wavevector mismatch for each case is $\Delta k = 0$. On the right is the fractional energy, defined as the energy of the component (signal or pump) divided by the sum (signal + pump). In the shaded region, there is significant measured parametric generation at the output of the PPLN crystal, indicating the seeded soliton is no longer stable. Parametric generation is not included in the beam propagation calculation; in the unshaded region where the contribution of parametric generation is negligible, the measured data agrees well with calculation.

The experimental data taken at soliton threshold is shown in Figure 14, and is compared with finite-difference beam propagation simulations of the continuous-wave coupled equations, assuming cylindrical symmetry in two transverse dimensions and averaged over a Gaussian temporal envelope to account for the time-varying power. The data shows reasonable agreement in the unshaded region. Parametric amplification of vacuum noise appears in the shaded region as a spectral peak at 1562 nm, far from the signal seed wavelength of 1553 nm and close to the phase-matching wavelength corresponding to the final QPM period. Similar experiments with uniform gratings at nonzero wavevector mismatch demonstrate that the soliton threshold increases sharply with wave-vector mismatch (positive or negative), and parametric generation is observed for $\Delta k < -125$ m^{-1} and $\Delta k > 750$ m^{-1}. This demonstrates a clear advantage of using chirped gratings over uniform gratings for obtaining tailored soliton output. This work has been submitted to was presented at the Conference on Lasers and Electro-Optics, 2005 in Baltimore, MD.

Ultrabroadband Parametric Amplification
We have investigated the use of chirped QPM gratings for high-gain, broadband optical parametric amplification. We have developed analytical and numerical methods to understand the amplification spectrum of these devices, and have obtained simple design rules. By way of example, an OPA using a 5-cm crystal of periodically-poled lithium tantalate together with a pump wave at 532 nm with an intensity of 5 GW/cm^2 can yield uniform gain of 10^5 over a bandwidth ranging from 630 to 900 nm, corresponding to a transform-limited pulse duration of 5 fs.

Although it allows tailoring of the gain spectrum through proper engineering of the chirp, a single QPM grating does not allow control of the phase response of the amplified signal wave. For applications such as short-pulse amplification, it is desirable to minimize the amount of group delay dispersion introduced by the amplifier, and if possible to have control over each dispersive order to prevent pulse distortion. This control can be obtained through the use of a tandem pair of gratings. As shown in Figure 15, this two-staged amplifier configuration uses the idler output of the first amplifier as the input signal of the second. By properly engineering the chirp of both QPM gratings, it is possible to achieve at the same time constant gain and constant group delay over large bandwidths. Figure 16-a and -b show the calculated gain and group delay spectra of such a tandem grating pair. The total gain between 680 and 800 nm is uniform and equal to 1.5×10^7, and the total group delay is also constant over that range. A paper describing the design of OPAs using chirped QPM gratings as well as the use of tandem gratings for simultaneous gain and group-delay control has been published in Optics Letters.[25]
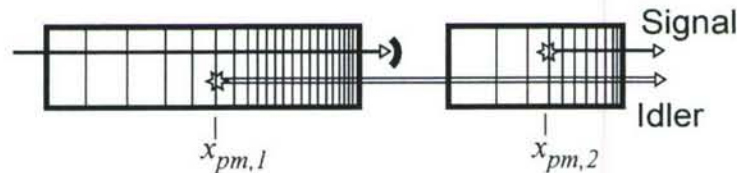

Figure 15 OPA using tandem chirped QPM grating for simultaneous gain and group-delay control.
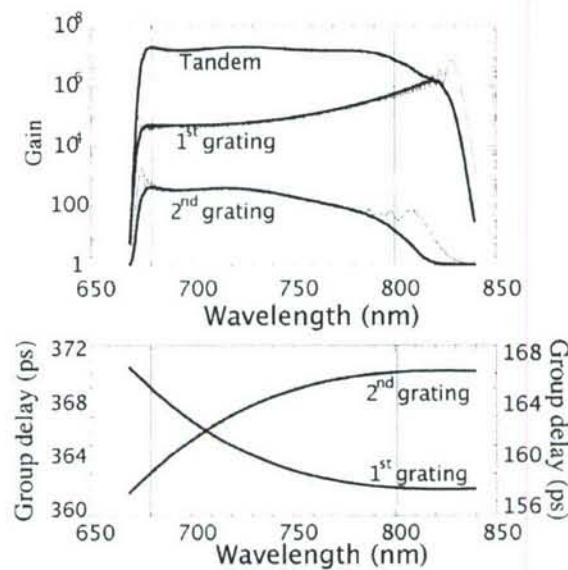
Figure 16. Design example of an OPA using tandem chirped QPM gratings. The gain (a, top plot) and group delay (b, bottom plot) spectra are constant over a bandwidth ranging from 680 to 800 nm.

II.3 Conclusions and Related Programs

This program has been highly successful in developing new devices based on the engineerable nonlinear optical materials, periodically-poled $LiNbO_3$, periodically-poled $LiTaO_3$, and OP-GaAs. It is worth noting that many of the devices developed are of direct relevance to DoD goals in general, and Air Force goals in particular. We anticipate that the next generation of advanced device studies based on these same two materials, which again pushes the envelope of what is currently practical, will follow a similar trajectory. (The follow-on program is currently funded under AFOSR Grant FA9550-05-1-0180.)

III. Supplemental Results on Ceramic Laser Development

R. Gaume, J. Wisdom, R. Feigelson, R. Route, and R. L. Byer

III.1 Introduction

Under DARPA contract DAAD19-02-1-0184, we producing and characterizing polycrystalline gain media for power scaling of high energy slab lasers. In this period, we have explored primarily the non-reactive sintering process as a method to produce low loss ceramic materials.

III.2 Progress

III.2.1 Background

Over the last decade, the requirements of high-power diode-pumped solid-state laser systems have presented a serious challenge for crystal growers. These lasers require crystals with greater size and greater homogeneity than has ever been demonstrated from single crystal growth. Practical high-power laser systems require doping profiles that efficiently and reliably couple low-brightness diode radiation into a structure with good overlap with a high-brightness signal beam. New processing technologies which limit the introduction of absorptive impurities are also needed. Ceramic

technology offers a dramatic advance toward efficient high-power laser systems by combining customizable doping profiles with fabrication scales limited only by the furnace size. One key aim of our ceramic laser development program is perform basic research into the fabrication of transparent ceramics with doping profiles and composite structures to enhance laser efficiency and reliability for power-scaling to high levels.

Within the developing transparent ceramics community, there are two recognized methods to attain laser grade materials, reactive and non-reactive sintering. As far as the preparation of transparent YAG ceramics are concerned, reactive sintering was the first method to achieve transparency. It amplifies the driving force behind densification by reacting precursor particles during sintering. For example, the three precursors powders shown below react during the sintering process to produce Nd:YAG,

$$xNd_2O_3 + 5Al_2O_3 + 3(1-x)Y_2O_3 \rightarrow 2(Y_{1-x}Nd_x)_3 Al_5O_{12}$$
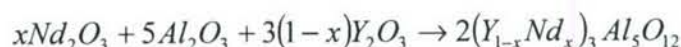
Last year we presented our progress in the fabrication of Nd:YAG using this method. While research on this process is still on-going, it has become apparent that non-reactive sintering will offer greater design flexibility.

In non-reactive sintering, nanoparticles of the desired phase are fabricated and formed into green bodies. In 2000, the Konoshima Chemical Corporation, collaborating with Professor Ueda of Tokyo University, succeeded in demonstrating a laser grade ceramic fabricated by non-reactive sintering. Today, highly transparent plates 10 cm by 10 cm in size have been fabricated for laser applications. Among the many advantages of this process is improved final homogeneity and easier patterning in the green state. We report our progress achieving transparency with these materials, as well as patterning them with micron-scale features.

III.2.2 Recent Developments

III.2.2.1 Non-Reactive Sintering Parameter Screening

In non-reactive sintering, a number of processing conditions, such as firing temperature and heating rate, are thought to influence the final transparency of oxide ceramics. To our knowledge, a quantified study has not been published of the influence of processing conditions on the final transparency of YAG ceramics. Our experimental plan was designed to screen through as many parameters as possible, and eliminate those with negligible impact on final ceramic transparency. A 2-level design of experiment (Plackett-Burnam scheme) has been carried out based on the five processing parameters listed in Table 2. This strategy allowed us to lower the number of parameters to be studied before going into a deeper investigation.

Processing Parameter	Value 1	Value 2
Powder Pre-Processing	Use as received	Decant in water 5 min
Green Ceramic Forming	Cold Isostatic Pressing	Slip Casting
Heating Rate	300°C/hr	600°C/hr
Final Dwell Temperature	1730°C	1780°C
Dwell Duration	3 hours	72 hours

Table 2 Various processing parameters in the design of experiment

Once sintered, cross-sections of the ceramics were cut and polished and ranked according to their optical quality. Optical quality was determined by measuring the size of macropores, the homogeneity of their distribution and the overall transparency.

The calculated mean effect for each of the five processing factors and factor combinations indicate that decanting the powder before use in conjunction with a moderate heating rate (300°C/h) lead to better results. To a lesser extent, the experimental data show the advantage of shaping green ceramics by slip-casting over cold pressing. These results emphasize the dramatic influence of the pore networks within the green ceramics on the achievement of transparency in sintered materials. For instance, the aggregates decantation that proceeds during the early stages of slip-casting is thought to be extremely favorable in leaving behind, a homogeneous slurry that will produce a dense compact by settlement. On the other hand, pressing powders might lock large pores in the green state due to high inter-particle friction. We are currently investigating the effect of different green ceramic shaping methods on the pore size distribution. Figure 17 shows the green ceramic pore size distribution for an isostatically pressed sample. Its bimodal shape reflects the different particle sizes used in this sample.
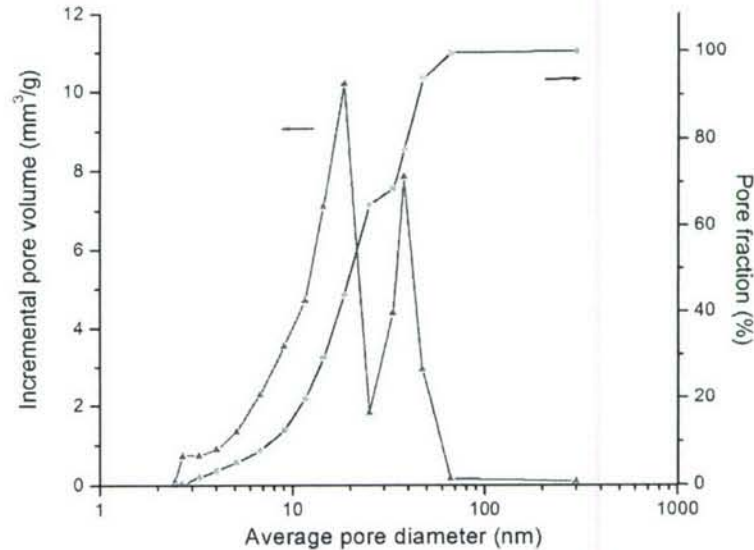

Figure 17 Pore size distribution in a green ceramic mixture of Y_2O_3+ Al_2O_3 (average particle sizes of 60 nm and 300 nm, respectively).

Another key parameter for transparency is the nanostructure of the powder itself. A laser grade ceramic requires a powder with the following essential characteristics: mono-dispersed particle size distribution, spherical shape, and very low agglomeration. Such powders yield higher densification and are less likely to experience anomalous grain growth during sintering. We have compared the sinterability of three commercial powders and Stanford-fabricated powders with the results shown in Table 3.

So far our best ceramic samples have been obtained using YAG nanopowders made at Stanford or with powders purchased from the Shin-Etsu company. The large polydispersity and the fair amount of powder agglomeration observed in the other powders are not favorable in making transparent samples.

Powder origin	MTI	Shin-Etsu	NEI	Stanford
Particle average size	ϕ=400 nm	ϕ=323 nm	ϕ=420 nm	ϕ=100 nm
Particle size distribution	100 <ϕ<2000 nm	270 <ϕ<386 nm	110 <ϕ<570 nm	40 <ϕ<110 nm
Multimodality	High	monodisperse	bimodal	monodisperse
Agglomeration	very high	moderate	high	Low
Sinterability	Poor	very good	moderate	very good
SEM pictures				

Table 3. Sinterability of various powders

III.2.2.2 Electrophoretic Deposition

We have been researching alternative forming methods to cold pressing and slip casting that offer the flexibility to make transverse patterns and gradients in ceramics. A promising method is electrophoretic deposition (EPD). EPD pulls nanoparticles from a dispersion, and deposits them on an electrode via a static electric field. This technique can yield green ceramic bodies of high density which may be sintered to transparency. When nanometer size powders are dispersed in a liquid phase, aggregation can be prevented by increasing particle surface charge or by adding polymeric dispersants which adsorb on the particle surface. Moreover, electrostatic repulsion and/or steric hindrance of the adsorbed polymer between adjacent particles lower the entropy of the particles packing once they settle. Therefore, processing ceramic slurries by EPD, pressure-casting, slip-casting or centrifugation generally lead to denser powder compacts than pressed powders.

The basic experimental setup of an electrophoretic deposition is shown in Figure 18. The first step is stabilizing the nanoparticles in the slurry against agglomeration. This is done by placing a charge on the surface of the nanoparticles by adjusting the pH and/or the salt concentration of the liquid phase. Once a stable slurry has been made, electrodes are inserted into the dispersion and a DC field is applied to cause migration and deposition of the nanoparticles to one of the electrodes. Once the particles reach the electrodes, they pierce through the charge cloud, and become attached to the electrode and each other.
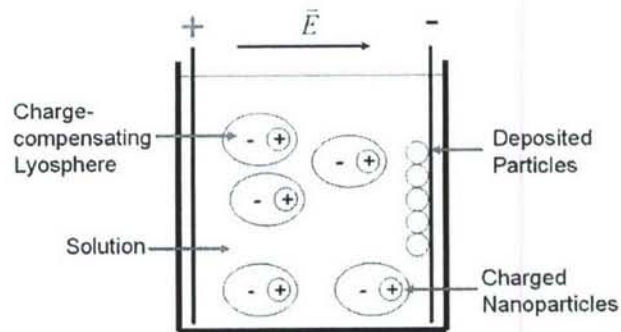

Figure 18. Schematic of a typical electrophorectic deposition

We have used this technique to deposit a YAG nanopowder on a gold electrode, achieving 64% of theoretical density. Figure 19a shows a sample before sintering and Figure 19b shows a sample after

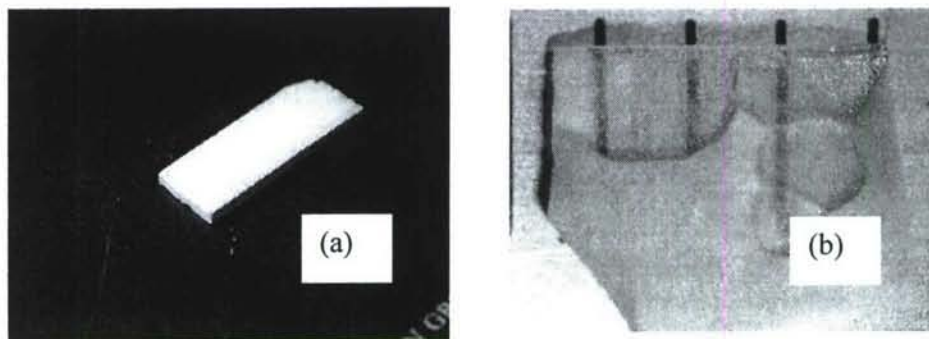sintering. The transparency is good in spite of anomalous grain growth, which often reduces transparency.

Figure 19. a) 2 cm long, 64% dense 1 at.% Nd:YAG green ceramic made by EPD
b) Single crystallization conversion in progress in a 400 μm-thick 1 at.%
Nd:YAG ceramic made by EPD and sintered at 1700 °C, 10^{-5} torr for 2.5 h

We have also begun investigations of transverse patterning on this sample. Our experiments used a single glass slide with two unconnected gold patterns which were held at different potentials. The electrode used in our experiments is pictured in Figure 20. The interlocking pattern of traces on the electrodes is such that adjacent traces are held at different potentials. The pitch (center spacing) of the traces was varied from 10 microns to 1mm. Three different pitch-to-trace-width ratios were also investigated. They indicated that small pitch to width ratios were more effective in forming microstructures with vertical features.

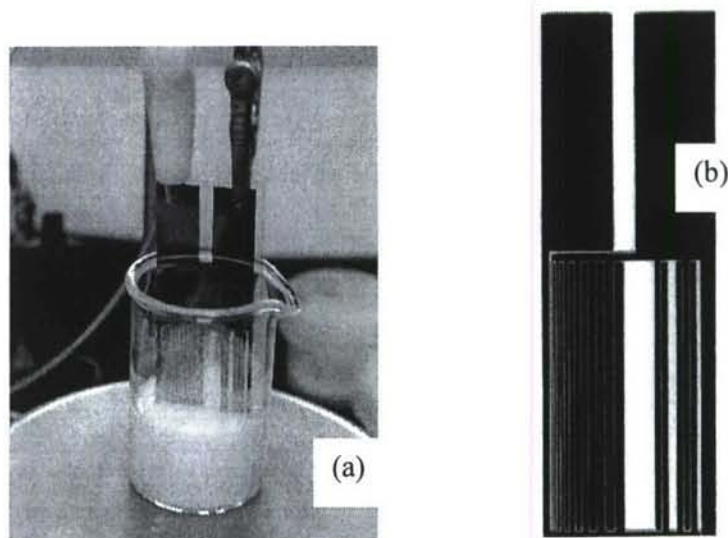
Figure 20. a) 1 at.% Nd:YAG slurry being deposited by electrophoresis. b) The layout of the electrodes used for green ceramic patterning. The clear section is the area with 10μm wide traces, separated by 100μm.

Pictured in Figures 21a and 21b are the results from several different strip sections. We have successfully shown that bar-like features can be fabricated at the 400 μm level, and even

demonstrated patterning at the 10 μm level, although the pitch-to-width-ratio did not favor vertical feature formation. We also were able to make a deposit on a carbon fiber, resulting in a hollow-core structure, after the sample was cooked in an oxidizing atmosphere. A deposit made on a 5 μm sample is shown in Figure 21c.
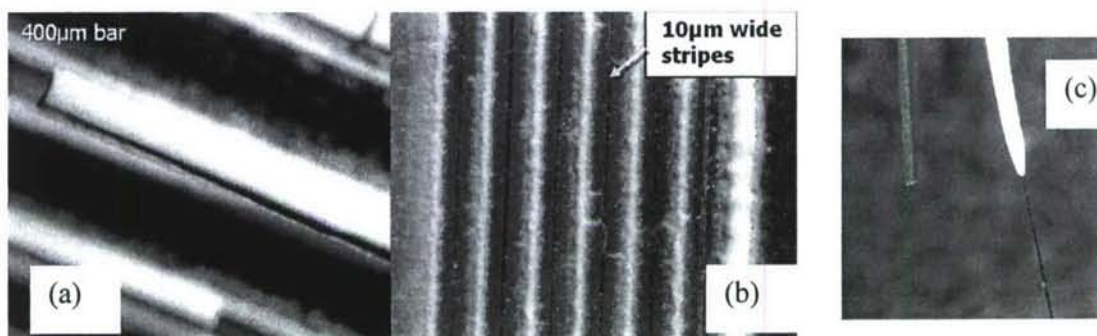

Figure 21. a) and b) Green ceramic microstructures fabricated by EPD, c) 7 cm by 30 μm OD by 5 μm ID Y_2O_3 green ceramic fiber made by EPD.

III.2.2.3 Micro-Imprinted Gratings

Another fabrication technique we have investigated is ceramic molding at the micron-scale. In molding process, a master mold is fabricated (in our case from silicon) and used to imprint a topological pattern onto a green ceramic body. The valleys of the impression can then be filled by a number of different ceramic processing techniques allowing sharp feature impressions, with two types of material. The value of this technique is that it leverages mature silicon micro-machining processes, offering submicron feature sizes. One potential application for this technique is the fabrication of high-power compatible transmission gratings (or for locations with high-levels of radiation).

We have successfully used micro-imprinting to pattern green YAG ceramics. Molds made of etched silicon consisted of 1 cm-long triangular parallel slits 5 to 20 microns deep. The clean features of this sample can be seen in Figure 22.

Figure 22. Stripes imprinted in a green YAG ceramic.

III.2.2.4 Nano-Engineered Ceramic Structures

One of the attractive potential benefits of ceramic gain media is the ability to engineer spatially varying doping profiles to enhance maximum output powers and improve laser brightness while improving efficiency. The most attractive avenue to fabricate transparent ceramics is by creating compositional gradients in the green ceramic by placing nano-particles with different compositions at various locations in the ceramic body, such that after sintering and densification the compositional profile results in the doping profiles desired. Numerous profiles with spatial features around 1 micron are interesting for laser applications. Such small profiles require precise positioning of precursor nano-particles to arrive at the profile of interest. While research into the fabrication of photonic crystals has demonstrated precise positioning of nanometer scale particles, an open question remains as to how well a nano-engineered doping profile will be transferred into a fully densified ceramic.

There are two intermediate steps between a nano-engineered compositional gradient and a fully densified ceramic. The first is shrinkage of the green ceramic as the free surface energy of the nano-particles (high surface curvature) is reduced. The second step is grain growth, as small numbers of residual pores are eliminated, but the length, width and height of the ceramic are essentially unchanged. The rate of these processes are mediated by the species with the lowest rate of volumetric diffusion, meaning that for every species doped in a ceramic, diffusion will play a significant role in the final profile shape. In addition to volume diffusion, mass transport of ions is increased by the presence of grain boundaries. Grain boundary diffusion occurs during both intermediate ceramic fabrication phases mentioned above, and depending on the time and the temperature of the process can smear out the profile of interest.

We have made measurements of the effective diffusion rates of Nd in transparent YAG ceramics with fine grains (~1 micron) in the temperature range of 1600°C to 1830°C. This is the equivalent of the second stage of the sintering process, where grain growth occurs to eliminate residual pores. The measurements were performed by taking an already transparent undoped YAG ceramic and diffusion bonding it to an already transparent 1 at.% Nd:YAG ceramic. Both of these ceramics were fabricated in Japan by Konoshima Chemical Co. After heat treatment, the Nd distribution was measured using a confocal microscope. The typical Nd concentration profile across the bonding interface is shown below..
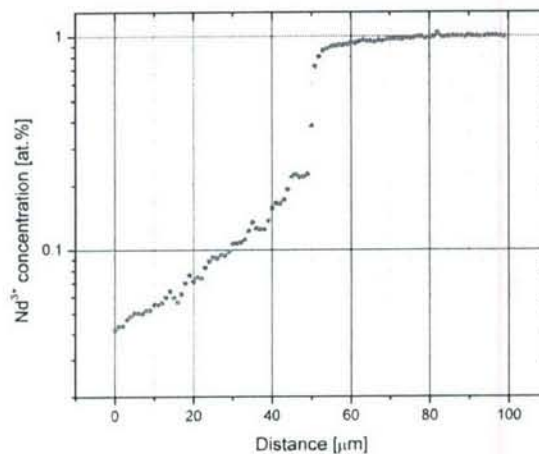

Fig. 23. Typical Nd concentration profile after diffusion bonding

Under the approximation of zero depletion of the 1 at.% Nd:YAG and following the formalism of LeClaire, we expected a concentration profile of the following form:

$$\frac{d \ln N(x)}{dx} = \frac{\Lambda(T)}{t^m}$$

where the coefficient $\Lambda(T)$ is a temperature dependant constant given by:

$$\Lambda(T) = C \exp\left[\frac{E}{RT}\right],$$

where R is the ideal gas constant and E is an effective activation energy of the process which is dependent on the grain boundary and bulk diffusion activation energies for Nd in YAG. The coefficient C is a combination of the defect densities of grain boundaries and the bulk material. In the temperature range of 1600-1750°C, we measured an activation energy of 420 kJ/mol, well below the measured activation energy for diffusion of Nd in bulk YAG made by Cherniak of 567 kJ/mol. The temperature range of 1750-1830°C the exponential dependence of $\Lambda(T)$ was eliminated by the process of grain growth. In this the range, we measured a fairly constant value of 0.2 μm-1h-1/2.

We are currently making measurements of Nd:YAG diffusion rates in single crystal material in the temperature range of 1700-1850°C in a reducing environment. With this data, we will be able to determine the required processing conditions for micron scale doping profiles. Understanding the interplay between grain boundary diffusion and volume diffusion of Nd will be important for high precision nano-structures as these profiles require very small (~10-50-nm) particle sizes. Such small particles sizes dramatically increase the number of grain boundaries in the material, and thus the effective mass transport of dopant out of the specified doping profile.

III.3 Future work on Ceramic Laser Development

We have compiled a number of different techniques to study powders, green ceramics and sintering parameters. We have used these techniques to improve the optical quality and reproducibility of our ceramics. We have initiated research to produce composite structures that will aid in pumping efficiency as well as functionality (for example integrated q-switches or bandwidth shaping doping profiles). Continuing research for future programs to address is recommended since these are key issues in the development of high energy laser systems.

III.4 Expenditures on Ceramic Laser Development

The main thrust of the supplemental award was to support the acquisition of major capital equipment for the fabrication of advanced ceramic laser host materials. Over the course of the supplemental award, we have acquired a high temperature vacuum furnace from Oxy-Gon Industries that is capable of high-vacuum operation to 2400° C and a hot isostatic press from American Isostatic Press that is capable of 30,000 psi operation at 2000° C. The balance of the supplemental award was used to support a post-doctoral affiliate who worked in support of the program.

IV. References

1. M. Katz, R.K. Route, D.S. Hum, K.R. Parameswaran, G.D. Miller and M.M. Fejer, "Vapor-transport equilibrated near-stoichiometric lithium tantalate for frequency-conversion applications", Opt. Lett. **29**, 1775 (August 2004).

2. D. H. Jundt, M. M. Fejer, and R. L. Byer, "Optical Properties of Lithium-Rich Lithium Niobate Fabricated by Vapor Transport Equilibration," *IEEE J. Quantum Electron.* **26**, 135 (1990)
   P. F. Bordui and R. G. Norwood, D. H. Jundt and M. M. Fejer, "Preparation and Characterization of Off-Congruent Lithium Niobate," *J. Appl. Phys.* **71**,875 (1991)
   D. H. Jundt and M. M. Fejer, R. G. Norwood and P. F. Bordui, "Composition Dependence of Lithium Diffusivity in Lithium Niobate at High Temperatures," *J. Appl. Phys* **72**, 3468 (1992)
   R. L. Holman, P. J. Cressman, and J. F. Revelli, "Chemical control of optical damage in lithium niobate," *Appl. Phys. Lett.* **32**, 280 (1978)

3. Y. Chen, J. Xu, Y. Kong, Sh. Chen, G. Zhang, and J. Wen, "Effect of Li diffusion on the domain inversion of LiNbO₃ prepared by vapor transport equilibration," *Appl. Phys. Lett.* **81**, 700 (2002)

4. Y. Furukawa, K. Kitamura, S. Takekawa, A. Alexandrovski, R. K. Route, M. M. Fejer, G. Foulon, "Improved material properties in MgO-doped near-stoichiometric LiNbO3 for nonlinear optical applications," CLEO 2000, Technical Digest. Postconference Edition. TOPS Vol.. 39, 7-12 May 2000, San Francisco, CA.

5. D.S. Hum, R.K Route, G.D. Miller and M.M. Fejer, "Quasi-phase-matched second harmonic generation using 42° rotated Y-cut near-stoichiometric lithium tantalate". CLEO 2004, May 2004, San Francisco, CA.

6. L. A. Eyres, P. J. Tourreau, T. J. Pinguet, C. B. Ebert, J. S. Harris, M. M. Fejer, L. Becouarn, B. Gerard, and E. Lallier, "All-Epitaxial Fabrication of Thick, Orientation-Patterned GaAs Films for Nonlinear Optical Frequency Conversion," *Appl. Phys. Lett.* **79**, 904-906 (August 2001).

7. T. Skauli, K. L. Vodopyanov, T. J. Pinguet, A. Schober, O. Levi, L.A. Eyres, M. M. Fejer, J. S. Harris, B. Gerard, L. Becouarn, E. Lallier, G. Arisholm, "Measurement of nonlinear coefficient of orientation-patterned GaAs and demonstration of highly efficient second harmonic generation," accepted to Opt. Lett.

8. K. L. Vodopyanov, O. Levi, P. S. Kuo, T. J. Pinguet, J. S. Harris, M. M. Fejer, B. Gerard, L. Becouarn, and E. Lallier, "Optical parametric oscillation in quasi-phase-matched GaAs", Opt. Lett. 29, 16 (2004).

9. P. S. Kuo, K. L. Vodopyanov, D. M. Simanovskii, X. Yu, M. M. Fejer, J. S. Harris, D.Bliss, D. Weyburne. Submitted to Conference on Lasers and Electro-Optics 2005.

10. G. Imeshev, M. M. Fejer, A. Galvanauskas, D. Harter, "Generation of dual-wavelength pulses by frequency doubling with quasi-phase-matching gratings," *Opt. Lett.* **26**, 268-70 (March 2001).

11. G. Imeshev, M. M. Fejer, A. Galvanauskas, D. Harter, "Pulse shaping by difference-frequency mixing with quasi-phase-matching gratings," *J. Opt. Sci. Am.* **B 18**, 534-39 (April 2001).
    G. Imeshev, M. A. Arbore, S. Kasriel, and M. M. Fejer, "Pulse shaping and compression by second-harmonic generation with quasi-phase-matching gratings in the presence of arbitrary dispersion," *J. Opt. Sci. Am.* **B 17**, 1420-37 (August 2000).

12. A. Galvanuskas, D. Harter, M. A. Arbore, M. H. Chou, and M. M. Fejer, "Chirped-Pulse-Amplification Circuits for Fiber Amplifiers, based on Chirped-Period Quasi-Phase-Matching Gratings," *Opt. Lett.* **23**, 1695-1697 (November 1998).

13. L. Gallmann, G. Steinmeyer, U. Keller, G. Imeshev, M. M. Fejer, J. P. Meyn, "Generation of sub-6-fs blue pulses by frequency doubling with quasi-phase-matching gratings," *Opt. Lett.* **26**, 616-16 (May 2001).

14. G. Imeshev, A. Galvanauskas, D. Harter, M. A. Arbore, M. Proctor, and M. M. Fejer, "Engineerable Femtosecond Pulse Shaping by Second-Harmonic Generation with Fourier Synthetic Quasi-Phase-Matching Gratings," *Opt. Lett.* **23**, 864-866 (June 1998).

15. O. E. Martinez, "Achromatic phase matching for second-harmonic generation of femtosecond pulses," *IEEE J. Q. Elec.* **25**, 2464-2468 (1989).
    A. V. Smith, "Group-velocity-matched three-wave mixing in birefringent crystals," *Opt. Lett.* **26**, 719-721 (2001)
    S. Ashihara, T. Shimura, K. Kuroda, "Group-velocity matched second-harmonic generation in tilted quasi-phase-matched gratings," *J. Opt. Soc. Am.* **B 20**, 853-856 (2003).

16. Jie Huang, J. R. Kurz, Carsten Langrock, A. M. Schober, and M. M. Fejer, "Quasi-group-velocity matching using integrated-optic structures," *Optics Letters* **21**, 2482 (2004).

17. R. Danielius, A. Piskarskas, A. Stabinis, G. P. Banfi, P. Di. Trapani, and R. Righini, "Travellling-wave parametric generation of widely tunable, highly coherent femtosecond light pulses," *J. Opt. Sci. Am.* **B 10**, 2222 (1993).

18. A. Galvanauskas, M. A. Arbore, M. M. Fejer, M. E. Fermann, and D. Harter, "Fiber-Laser-Based Femtosecond Parametric Generator in Bulk Periodically Poled LiNbO3," *Opt. Lett.* **22**, 105-107 (January 1997). M. L. Bortz, M. A. Arbore, and M. M. Fejer, "Quasi-Phasematched Optical Parametric Amplification and Oscillation in Periodically-Poled LiNbO3 Waveguides," *Opt. Lett.* **20**, 49–51 (January 1995).

19. A. Galvanauskas, M. A. Arbore, M. M. Fejer, M. E. Fermann, and D. Harter, "Fiber-Laser-Based Femtosecond Parametric Generator in Bulk Periodically Poled LiNbO₃," *Opt. Lett.* **22**, 105-107 (January 1997).

20. Xiuping Xie, Andrew M. Schober, Carsten Langrock, Rostislav V. Roussev, Jonathan R. Kurz, Martin M. Fejer, "Picojoule threshold, picosecond optical parametric generation in reverse proton-exchanged lithium niobate waveguides", *JOSA* **B 21**, 1397-1402 (July 2004).

21. G. P. Banfi, P. Ditrapani, R. Danielius, A. Piskaraskas, R. Righini, and I. Santa, "Tunable femtosecond pulses close to the transform limit from traveling-wave parametric conversion," *Opt. Lett.* **18** pp. 1547-1549 (September 1993).

22. A. Galvanauskas, A. Hariharan, and D. Harter, "High-Energy Femtosecond Pulse Amplification in a Quasi-Phase-Matched Parametric Amplifier," *Opt. Lett.* **23**, 210-212 (1998).

23. A. Galvanauskas, A. Hariharan, F. Raksi, K. K. Wong, D. Harter, G. Imeshev, and M. M. Fejer, "Generation of diffraction-limited femtosecond beams using spatially-multimode nanosecond pump sources in parametric chirped pulse amplification system," CLEO, 2000, CThB4.
S. Carrasco, J. P. Torres, L. Torner, and M. M. Fejer, "Efficiency-enhanced Soliton Optical Parametric Amplifier," *JOSA* **B 19**, 1396-1400 (2002).

24. L. Torner, C. B. Clausen and M. M. Fejer, "Adiabatic shaping of quadratic solitons," *Opt. Lett.* **23**, 903-905 (1998).

25. M. Charbonneau-Lefort, M.M. Fejer, and B. Afeyan,"Tandem chirped quasi-phase-matching grating optical parametric amplifier design for simultaneous group delay and gain control", Optics Letters, No. 30 Vol. 6 pp.634 (March 2005)